THE JOURNAL OF PHYSICAL CHEMISTRY B

Article

pubs.acs.org/JPCB

Molecular Dynamics Investigation of Ion Sorption and Permeation in Desalination Membranes

Vesselin Kolev and Viatcheslav Freger*

Wolfson Department of Chemical Engineering, Technion, Haifa 32000, Israel

Supporting Information

ABSTRACT: With the purpose of gaining insights into the mechanisms of ion uptake and permeation in desalination membranes, MD investigation of a model polyamide membrane was carried out. A relatively large membrane (45K atoms) was assembled, which closely matched real desalination membrane in terms of chemistry and water permeability. Simulations demonstrate that the mechanism of ion uptake distinctly differs from mean-field approaches assuming a smeared excluding Donnan potential. Ion sorption on charged sites in the membrane phase appears to be highly localized, due to electrostatic forces dominating over translational entropy. Moreover, sorption on partial atomic charges becomes possible as well, which greatly enhances salt (co-ion) uptake and weakens the effect of fixed charges on salt exclusion. This could explain high ion uptake measured in polyamide membranes for both co- and counterions and variations of ion sorption and permeation at low salt concentrations. On the other hand, present simulations greatly overestimate ion permeability, which could be explained by a more open structure than in real membranes, in which dense polyamide fragments may efficiently block ion permeation. Unfortunately, MD cannot analyze ion uptake and permeation in dense fragments containing too few ions, which calls for new approaches to studying barrier properties of polyamide.

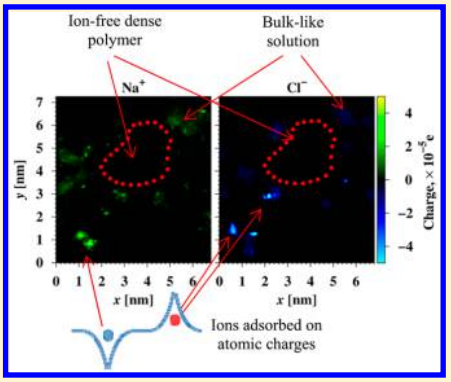

1. INTRODUCTION

Thin-film composite membranes of reverse osmosis (RO) and nanofiltration (NF) types are widely used today in desalination, purification, and recycling of various aqueous streams.[1,2] These membranes have a polyamide selective layer obtained by interfacial polymerization (IP), a complex film-formation process that produces a film with inherent nanoscale variations of porosity and chemistry.[3,4] Much effort has been invested in understanding membrane structure and its relation to selectivity and permeability;[1,3−18] however, many questions are still open.

Over the past years, there has been significant progress in applying to this problem the methods of molecular dynamics (MD).[19−25] Recently, our group presented a molecular model of polyamide[26] composed of 44 467 atoms and 237 ionizable COOH groups that was thoroughly assembled through a random condensation protocol to closely match available Rutherford backscattering spectroscopy (RBS) and other data on chemical composition and cross-linking of polyamide.[14] This was an improvement over previous MD studies that utilized significantly more charged and less cross-linked and hence less rigid structures. The model was used to analyze porosity, swelling, uptake of water, and water diffusion within polyamide, which showed a reasonable agreement with available experimental data.

It must be emphasized that the exact structure of the polyamide membranes is still not known well, even though the overall thickness and average chemical composition, matched by the present model, are relatively well-determined. The reasonable agreement between published MD simulations, including our previous study, and experimental values of water content and permeability might be somewhat fortuitous and simply result from small sensitivity of water permeation to microstructural details. This might not be the case for salt permeation; however, MD results on salt permeation are scarce and less conclusive.

The main motivation and purpose of this study was therefore to extend the MD simulations to analysis of transport and uptake of salt and individual ions. A special emphasis is placed here on the role of nanopores and fixed charges, inherent to polyamide structure, and the relation to salt exclusion and transport. The localized effects in nanopores and around fixed charges are the most difficult to treat within analytical models of salt exclusion and permeation, which are usually of the mean-field type and assume that average or effective characteristics, such as a uniform Donnan potential or smeared surface charge, can be applied to the entire membrane phase or nanopore surface. Deviations from such mean-field concepts are where MD can supply a crucial insight, unavailable at present through other research tools. Apart from this insight into the mechanism of salt exclusion and applicability of mean-field concepts, another purpose of this study was to clarify whether the simulated polyamide structure can provide quantitative

Received: July 8, 2015
Revised: September 17, 2015

DOI: 10.1021/acs.jpcb.5b06566
J. Phys. Chem. B XXXX, XXX, XXX−XXX

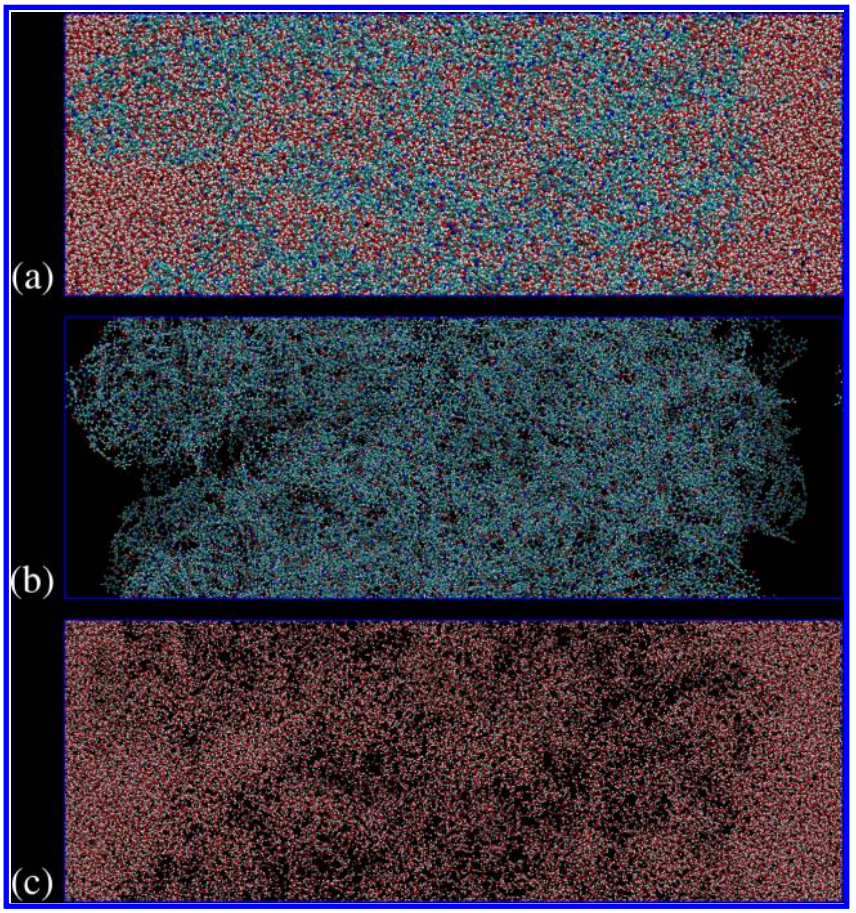

Figure 1. *yz* projected view of the simulation box and its content, as assembled previously:[26] (a) entire content, (b) polyamide only, (c) water only.

estimates for salt permeability and partitioning of salt and individual ions consistent with experimental observations.

2. SOFTWARE, HARDWARE, MOLECULAR MODELS, SIMULATION PROTOCOLS, AND DATA POSTPROCESSING

2.1. Software and Hardware. All MD simulations were performed by running GROMACS[27−31] package, version 5.0.4 with GPU support. Its source code was compiled with Intel C++ Compiler XE 15.0.0 (GCC version 4.4.7 compatibility) for Linux (x86_64) with GPU support against CUDA 7.0 libraries, to achieve better performance. A workstation equipped with 2 × Intel Xeon X5650 CPU and 1 × NVidia Tesla K20 GPU running CentOS 6.6 (Linux kernel 2.6.32, Intel 64) was employed as a computing node. The molecular topology of the polyamide molecule was stored and edited in SQLite (3.6.20) database. The spatial distribution of the atomic mass, charge, and velocity across the simulation box was collected by processing the trajectories recorded by GROMACS. That was assisted by an analysis tool set written in Fortran 2003 (Intel Fortran Compiler XE 15.0.0 for Linux was used to produce the linkable binary code) and linked as modules within Python 2.7 scripts. Xdrfile code (supplied by GROMACS project) was also adopted as a binary Python module in order to read the frames one by one directly from the trajectories.

2.2. Model Polyamide, Water, Ions, and Force Field. Assembly of the model polyamide molecule was reported previously.[26] The molecule consisted of 44 467 atoms (394 568.898 amu), and its molecular topology (atomic types and charges, bonds, and improper dihedral angles) followed the parametrization provided by the GAFF force field.[32] In this study the TIP3P water model[33] was replaced with SPC[34] (see section S1 in Supporting Information for details), since it reportedly better represents the solvent properties in systems with interfaces,[35] yielding a more contrasting spatial distribution of the water dipoles at the interface. The used GAFF force field parameters for Na^+ and Cl^- are those published by Chen and Pappu.[36]

2.3. Simulation Protocols. The swollen polyamide molecule and its ionized form were settled inside a prismatic simulation boxes with sizes ∼6.8 nm × 7.2 nm × 20 nm, as shown in Figure 1. Periodic boundary conditions (PBC) in all dimensions were applied to create a polyamide membrane of an infinite surface area. The following simulation protocols were consecutively applied to the simulation box content: (a) settling, (b) salination, (c) ionization (for fully ionized membrane only), and (d) equilibration. They are described in detail along with their GROMACS start configurations (which include all parameters of the simulations) in sections S2−S5 of Supporting Information. The salination protocol was not only used to introduce salt to the system but also supplied reference data for 0.5 M NaCl solution. The goal of the ionization protocol was to convert all 237 COOH groups into COO^- fixed charges and to obtain a fully ionized membrane. It must be stressed that, as a result of salt redistribution between the bulk solution and membrane phases, the equilibrium NaCl concentration in solution differed from the initially introduced 0.5 M, which was taken into account in the analysis of salt permeability and ion partitioning.

DOI: 10.1021/acs.jpcb.5b06566
J. Phys. Chem. B XXXX, XXX, XXX−XXX

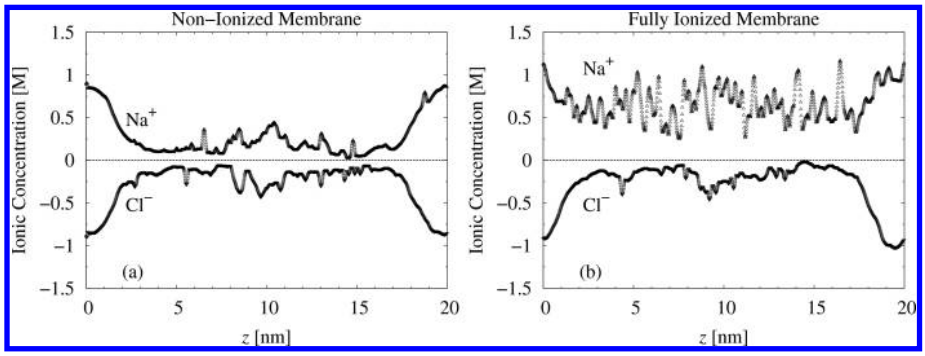

Figure 2. Distribution of the total Na^+ and Cl^- ionic charge along the samples of (a) nonionized and (b) fully ionized polyamide membranes expressed as molar concentrations within a probing slice of thickness $\Delta z = 0.167$ nm moving in the z-direction of the simulation box in $\delta z = 0.0151$ nm steps.

To correctly measure and analyze the atomic velocities, the barostat algorithm in the equilibration protocol was changed from Berendsen[37] to Parrinello–Rahman[38,39] (section S5 in Supporting Information). Note that the productive stage of the simulation, which was part of the equilibration protocol used for the computing of the results, was 200 ns long.

2.4. Data Postprocessing. The spatial distribution of the atomic charge and velocity were calculated by means of the dedicated analysis tool set based on the grid statistics, as described in detail in section S6 of the Supporting Information. Grids of 450 × 480 × 1325 nodes were constructed to analyze spacial distribution of different physical properties within the simulation box. To analyze distribution of average properties across the membrane the simulation box was scanned with a moving slice of dimensions 6.8 nm × 7.2 nm × 0.167 nm that was moved in z direction by $\delta z = 0.015$ nm steps. The thickness of the probing slice (0.167 nm) was optimized as described in section S6.3 of Supporting Information, while the 0.015 nm step was the spacing between 1325 nodes in z direction.

The calculation of the radial distribution functions (RDF)[38] and self-diffusion coefficients, D, was obtained by means of the GROMACS tools g_rdf, and g_msd. They were calculated for the "active part of the membrane": the part of the simulation box where the spatial atomic charge distribution is representative for a bulk polyamide membrane (see next).

3. RESULTS AND DISCUSSION

3.1. Ionization, Hydration, and Ion Sorption. The large (about 45K atoms) polyamide molecule assembled previously from *m*-phenylenediamine (MPD) and trimesoyl chloride (TMC) monomer was used in this study to assemble a hydrated membrane facing an aqueous salt solution at both sides, as shown in Figure 1. Given that the microscopic polyamide structure is not regular, its relatively large size allowed collecting fairly robust statistical averages of main characteristics of interest, without imposing unrealistic demands on computational time and resources. The size was particularly important for analyzing fixed charges and ions in the system, which are relatively scarce species even for the relatively concentrated NaCl solution used here.

The polyamide molecule building up the membrane contained 237 weakly acidic carboxylic groups, i.e., about 7 such groups per 100 amide bonds, which in a real membrane, depending on the specific pH, would be partly or fully ionized in water. Unfortunately, the ionization degree cannot be deduced from MD simulations, nor can it be *a priori* specified for a given pH, since this depends on the yet unknown pK_a of the acidic groups. Although pK_a in water is known, in an organic or polymeric phase it would depend on the dielectric constant and, in the present case, could vary between locations, depending on the local hydration. As ionized groups tend to be more hydrated than nonionized ones, ionization and hydration must be interrelated in a complex way. Nevertheless, it was not clear how much difference the ionization would make. To understand its relative importance, we chose to simply consider two limiting cases whereby all fixed charges are either completely associated, i.e., the polymer is overall electrically neutral, or completely dissociated (ionized); thus, the polymer bears a maximal fixed charge. In the latter case this charge had to be neutralized by Na^+ counterions when the membrane was equilibrated with a NaCl solution to ensure electroneutrality.

It must be stressed that the other atoms of polyamide, especially O and N of the amide groups, may bear significant partial atomic charges as well. These charges were initially computed for MPD and TMC monomers and MPD-TMC dimers using RESP routine[40,41] and redistributed in the course of polymerization and formation of amide bonds, which further reduced the partial charges of O and N atoms.[26] These charges then do not interact with water and ions as strong as fixed charges, and their overall net charge is zero. Nevertheless, they may have a substantial impact on the dynamic and equilibrium properties of the system, as revealed by analyzing the two simplified ionization scenarios.

Figure 2 shows the spatial atomic charge distribution of Na^+ and Cl^- across the membrane, computed by grid analysis (section S6 in Supporting Information). Each point represents the average amount of the atomic charge associated with a particular ion located in the probing slice (see section 2.4) at certain z. Disregarding fluctuations, the profiles plateau in the region $3 \le z \le 17$, representing and thereafter referred to as the inner bulk of the membrane, while the complementary regions $z < 3$ and $z > 17$ are treated as outside regions, even though they contain some polymer as well, except for the special region $18 < z < 19$ nm containing only the solution phase. For the neutral membrane the total charges borne by Na^+ and Cl^- are exactly compensated, and small local mismatches reflect fluctuations of the local charge. On the other hand, for the charged membrane the total charges borne by Na^+ and Cl^- ions differ by the total negative fixed charge of the membrane ($237e$), and the Na^+ profile fluctuates more strongly due to the occasional presence of discrete fixed charges within some slices.

Maps in Figure 3 explicitly show time-averaged distribution of atomic charge for ionized and neutral membranes within representative slices at $z = 6.2$ and 19.1 nm, i.e., inside and just

DOI: 10.1021/acs.jpcb.5b06566
J. Phys. Chem. B XXXX, XXX, XXX–XXX

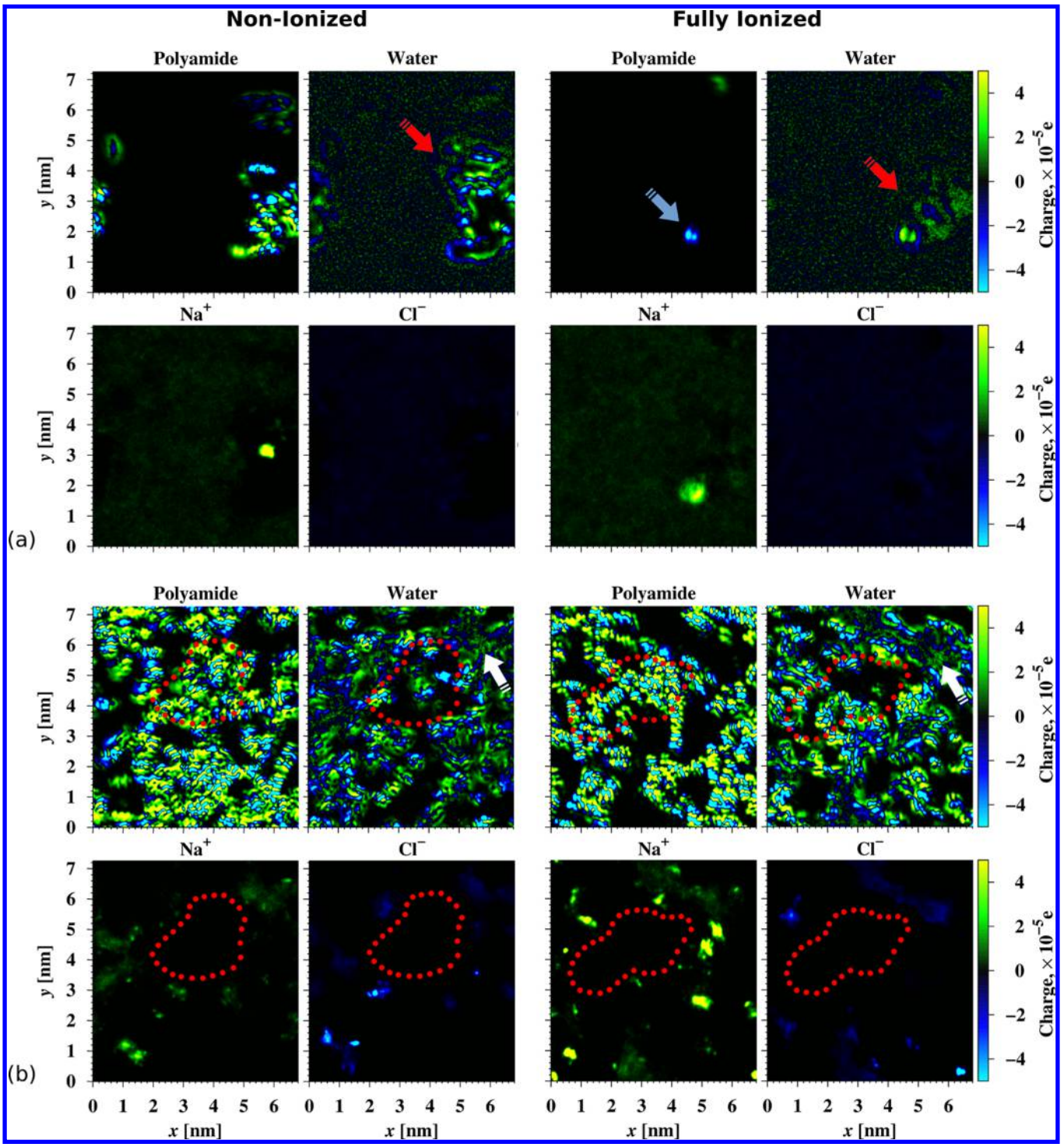

Figure 3. Time-average distribution of the atomic charge of the polyamide, water, Na^+, and Cl^- ions across an *xy* slice of thickness Δz = 0.167 nm: (a) just outside the membrane next to water/polyamide interface at z = 19.1 nm and (b) deep inside the membrane at z = 6.2 nm. The left half corresponds to the nonionized membrane and the right half to the fully ionized membrane. Blue arrow indicates a single COO^- charge of polyamide protruding into solution. Red arrows indicate water aligned next to the polyamide−water interface. White arrows indicate bulk-like water within large voids inside polyamide. Regions encircled with a red dashed line indicate dense polyamide fragment. (See Supporting Information section S6 describing the statistical routine and plotting technique and video files.)

outside the membrane, for 4 species: polyamide, water, Na^+, and Cl^-. Perhaps the most striking feature is the strong immobilization and alignment of water next to atomic charges of polyamide, whose charge pattern sustains over time and does not fluctuate significantly. Similar water structuring effects in nanopores, neutral and charged, were reported in many other studies.[42−45] Water panels in Figure 3a shows that while water in solution outside the membrane and far enough from the interface is featureless, water molecules just next to polyamide (designated with red arrows) are immobilized and form a distinct charge distribution pattern that sustains as well. Figure 3b shows that inside polyamide water molecules lining the

DOI: 10.1021/acs.jpcb.5b06566
J. Phys. Chem. B XXXX, XXX, XXX−XXX

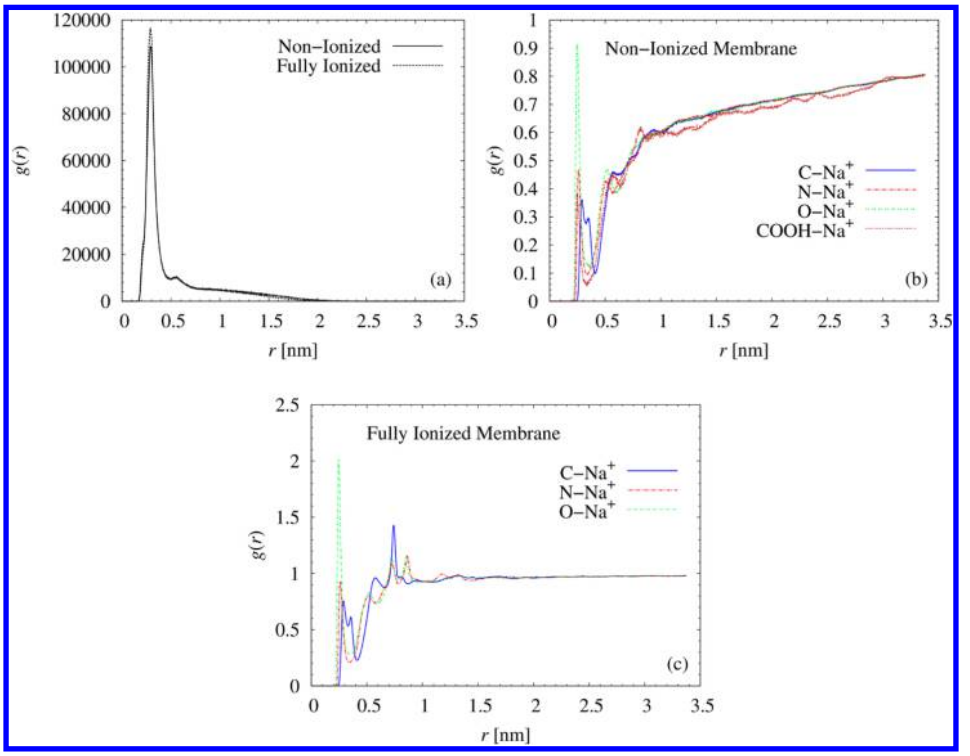

Figure 4. Computed radial distribution functions $g(r)$ showing correlations between (a) the center of the mass of SPC water molecules and the polyamide chain; (b) C, N, and O atoms and undissociated COOH groups of neutral polyamide membrane and Na^+ ions; (c) same as part b for the fully ionized membrane. The plots are representative of the inner part of the membrane.

inner pore surface are immobilized in a similar manner and only a small fraction found in largest cavities appears as featureless as the bulk solution (designated with white arrows). Figure 4a displays the radial distribution function (RDF) between water and polyamide, in which C, O, and N making up the polyamide structure are viewed collectively as a single type of atoms. The large peak at ∼0.3 nm indicates a strong alignment of the first layer of water next to the water−polyamide surface and little structure beyond that layer. These patterns show no significant difference for ionized and neutral membranes.

Similar to that of water, maps of Na^+ and Cl^- densities in Figure 3 show that in the bulk solution (outside the membrane) the ions have a fairly uniform density; however, within polyamide they concentrate in strongly localized spots. In the neutral polymer the spots of Na^+ and Cl^- are correlated to some degree, but in some locations ions of one type only are found, pointing to the existence of either positive or negative fixed charges attracting oppositely charged ions. These localized spots may be viewed as a 3D analogue of the well-known localized and immobilized 1D layer of counterions, the Stern layer, next to a charged interface in solution.[46] More of them and significantly more Na^+ than Cl^- is seen in the ionized membrane due to the presence of ionized COO^- groups. One such spot of Na^+ around a COO^- charge just at the polyamide−water interface extending to the adjacent solution is also seen in Figure 3a marked with a blue arrow. In contrast, well-correlated, smeared, and nearly uniform clouds of both Na^+ and Cl^-, resembling the bulk solution, are observed in relatively large pores, in which a bulk-like structureless water is present as well.

The RDF correlation between Na^+ ions and oxygen atoms of COO^- groups (not shown) displays peaks at 0.226 and 0.431 nm, indicating formation of contact (CIP) and solvent-separated (SSIP) ion pairs, respectively, with a peak ratio ca. 32:1. The high ratio of the primary and secondary COO^- charges once again indicates a strong attraction of Na^+ counterions in polyamide, quite different from the more diffuse cloud shape obtained by Aparicio and Atilhan[47] next to Ar−COO^- groups in solution. The ion separation in CIPs 0.226 nm should be roughly the size of a Na^+ spot. Given the fact that there are 237 fixed charges spread over a 14 nm thick membrane, the Na^+ map in the right plane of Figure 3b is supposed to contain of the order of $237 \times 0.226/14 \approx 4$ Na^+ spots associated with COO^- charges, which is consistent with the observed number of most intense spots.

However, in Figure 3b there are clearly other spots, not associated with ionized carboxylic groups, to which ions get attracted, though perhaps not as strongly as to fixed charges. This is most obvious for nonionized membrane, in absence of any genuine fixed charges (Figure 3); however, localization of Cl^- at some location in the negatively charged ionized membrane is another strong indication. Some Cl^- and Na^+ clouds are complementary, but some are not, or the correlation between the two is weak, as seen in Figure 2. The quite featureless radial distribution functions RDF in Figure 4b,c emphasize that this is not a general correlation between the polyamide atoms and ions analogous to the polyamide−water correlation in Figure 4a. Rather, ions are attracted to just a few specific locations. We believe that this result highlights attraction to partial atomic charges in the polyamide matrix, which is sustained over time due to the rigid structure of polyamide. Even if the polymer is overall neutral, the local atomic charges may provide enough attraction energy to localize an ion to a substantial degree, provided there is enough separation of positive and negative atomic charges to create a sufficiently strong local electric field at typical interionic

DOI: 10.1021/acs.jpcb.5b06566
J. Phys. Chem. B XXXX, XXX, XXX−XXX

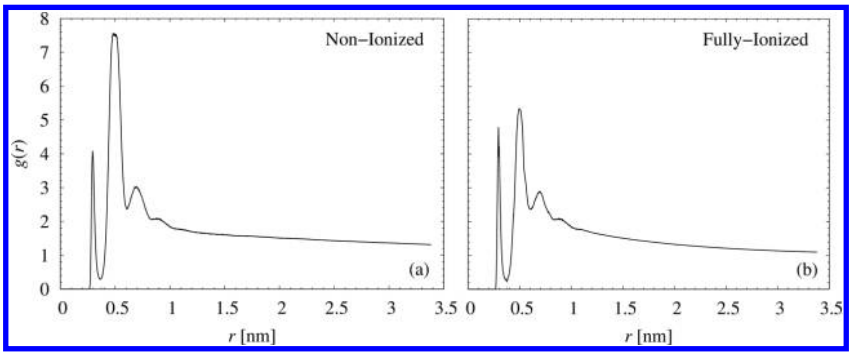

Figure 5. Radial distribution function between Na^+ and Cl^- inside (a) the nonionized and (b) ionized membrane.

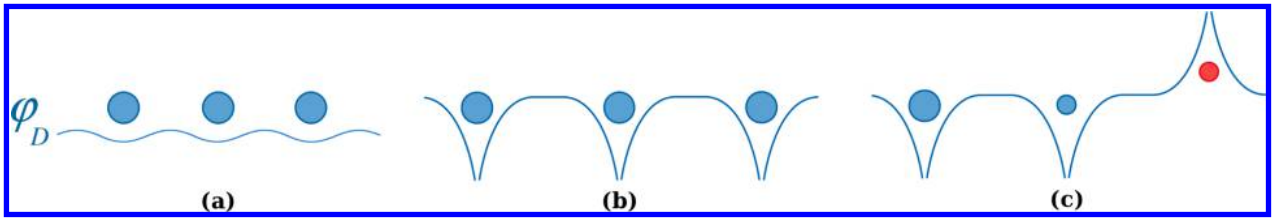

Figure 6. Schematic illustration of different ion sorption regimes: (a) the Donnan model, λ_B is small compared to charge spacing, negative fixed charges collectively exert a negative nearly uniform Donnan (φ_D) on the entire membrane phase; (b) the localized sorption regime, λ_B is large compared to charge spacing, negative fixed charges form separate potential wells trapping mobile ions; (c) localized sorption involving both genuine fixed charges and "active" partial atomic charges of the same as well as opposite sign (minority charges). Large filled circles designate genuine negative fixed charges; smaller circles designate atomic charges, positive (red) and negative (blue). Solid lines schematically depict potential variations; mobile ions are not shown.

distances. For instance, the relative intensities of the first peak of RDFs in Figure 4b,c indicate that average attraction of Na^+ to electronegative O atoms is distinctly stronger than to C or N. Such well-separated charged atomic sites are relatively sparse, but even a small amount could strongly affect ion sorption. This type of ion−polyamide interaction has not been explicitly considered in previous simulations; however, it was postulated in some phenomenological models.[48]

The sorption to such atomic charges rather than genuine fixed charges could explain unexpectedly high ion sorption in polyamide membranes measured by Zhang et al. using RBS,[49] which seemed inconsistent with the high salt rejection by polyamide. While polyamide is supposed to exclude ions, the measured ion partitioning coefficients K were larger than 1; i.e., there were more ions in polyamide than in water. The measured sorption was also not much different for counter- and co-ions, suggesting it was unrelated to the membrane fixed charge. A similar high sorption of salt in neutral aliphatic Nylon with $K > 1$ was also reported by Toubeli and Kiparissides.[50]

Figure 5 showing RDF between Na^+ and Cl^- ions offers another insight into interionic interactions in polyamide. Compared to bulk solution,[51,52] the CIP peak at ∼0.3 nm is largely suppressed while the SSIP one at ∼0.5 nm is enhanced, more in the neutral membrane. The CIP peak may be associated with the interaction of free Na^+ and Cl^- in large pores, similar to bulk solution, for which this peak should be dominant.[51,52] Dominance of SSIP peak in Figure 5 may be explained by sorption on fixed or atomic charges, in which case Na^+ and Cl^- have to form a triplet with a charged site rather than a pair and Na−Cl attraction will be weaker. This mechanism may also explain why SSIP is reduced for an ionized membrane; this may come from the fact that zero net charge of a COO^-Na^+ pair should attract a Cl^- less strongly than Na^+ adsorbed on a partial atomic charge.

Bason et al. pointed out that permeability of salt in semiaromatic polyamide NF membranes, known to possess fixed charges, tends to become independent of salt concentration in dilute feed solutions, opposite to what is expected for a charged membrane based on the Donnan or combined Steric−Donnan−diElectric (SDE) exclusion model.[53,54] Recently, Galama et al.[55] demonstrated that ion sorption in ion-exchange resins obeys a model analogous to SDE in a wide salt concentration range; however, co-ion sorption at low concentrations shows a discrepancy similar to the one observed by Bason et al. The only plausible way to explain this result was to assume the presence of minority fixed charges opposite to the dominant fixed charge. The present observations suggest that atomic charges, sufficiently separated from adjacent opposite atomic charges, may play the role of such minority charges.

It may be noted that low dielectric properties of the polymer may amplify this effect. To see it most transparently, one may consider the Bjerrum length of the medium λ_B, which sets the scale below which electrostatics dominates over thermal energy k_BT, as follows:[54]

$$\lambda_B = e^2/4\epsilon\epsilon_0 k_B T \quad (1)$$

Here, e is the electron charge, and ϵ is the dielectric constant of the medium. When the spacing of fixed charges exceeds λ_B, the thermal motion (or translational entropy) of the ions is negligible compared to electrostatic forces and unable to uniformly spread the ion across the membrane phase, as it does in aqueous solutions and as assumed in the Donnan and SDE models. This invalidates the concept of a single and uniform Donnan potential that is exerted collectively by all fixed charges together on all ions in the membrane phase (Figure 6a). Instead, fixed charges form deep and well-separated potential wells thus fixed, and mobile charges mainly interact pairwise

DOI: 10.1021/acs.jpcb.5b06566
J. Phys. Chem. B XXXX, XXX, XXX−XXX

(Figure 6b). As a result, mobile ions strongly adsorb on fixed charges. The small translation entropy allows the counterions to move only over a limited space around the fixed charge; thereby, the adsorbed ion becomes highly localized (cf. ion spots in Figure 3b). Moreover, due to strong localization, the adsorbed counterion nearly fully neutralizes the fixed charge. Thereby, its potential barely affects other mobile ions in the system, again, invalidating the concept of a single Donnan potential collective exerted by all fixed charges.

A notable feature of the Donnan scenario is that the atomic charges must exactly cancel out in the overall (background) fixed charge and play no role. However, in the just described localized sorption scenario, individual atomic charges may well act as individual and independent adsorption sites for one type of ion (Figure 6c). The mean dielectric constant of hydrated polyamide ε is probably under 10, given the refractive index of dry polyamide is $\varepsilon^{1/2} \approx 1.7$,[56] i.e., $\varepsilon \approx 3$, and that of confined water is less than 15% of bulk value, i.e., less than 12.[25] For such ε and univalent ions ($z_e = 1$) λ_B should then exceed 5 nm, which is indeed much larger than the spacing of ion spots in Figure 3b. Even though for atomic charges $z_e < 1$ and λ_B must be shorter, for some "active" atomic charges it may still be sufficiently large to lead to the localized sorption. Remarkably, in the case of a charged membrane, atomic charges of the same sign as genuine fixed charges may pass unnoticed, but opposite atomic charges will show up as minority charges and result in a finite salt sorption at very low salt concentrations, as Galama et al.[55] indeed observed. In a neutral membrane, they may also set minimal salt sorption C_s, especially, in a low dielectric membrane, in which ion solubility would be low without such charges. In such cases apparent salt partitioning $K_s = C_s/c_s$ will increase when salt concentration c_s decreases, as was observed in RBS experiments of Zhang et al.[49]

3.2. Dynamics of Ions and Water. Dynamics of water and ions inside polyamide provides another insight into the state of these species in the membrane. One such characteristic is the distribution of ion velocities. The GROMACS tool set computes this distribution by tracing atomic velocities, i.e., based on the simulation trajectories. However, in order to compare the ion velocities inside and outside the membrane and map them in a manner similar to atomic charge maps in Figure 3, the spatial distribution of time-averaged ion velocities on a 3D grid was computed, as elaborated in section S6 in Supporting Information, which also ensured that atom trajectories-based and grid-based statistics yielded identical velocity distribution for the entire membrane.

The appropriate overall characteristics that may be compared for selected spatial regions are the probability mass function (PMF) of the atomic velocities, $p(v)$, as well as the most probable velocity, v_p, and the root-mean-square (RMS) velocity, v_{rms}, that may serve as appropriate metrics and are defined as follows:

$$\frac{dp(v)}{dv} = 0 \text{ at } v = v_p \tag{2}$$

$$v_{rms} = \left(\int_0^\infty v^2 p(v)\, dv\right)^{1/2} \tag{3}$$

Figure 7 shows the distribution $p(v)$ inside and outside the nonionized and ionized membranes, and Table 1 displays v_p and v_{rms} calculated for the Na^+ and Cl^- ions in the specified regions. These characteristics are compared with 0.5 M NaCl bulk solution obtained as part of the salination protocol. It is seen that v_p is essentially identical inside and outside the membrane and in the bulk solution. On the other hand, v_{rms} differs significantly and increases inside the membrane, compared to 0.5 M NaCl solution. Note that in the classical Maxwell distribution v_p and v_{rms} are rigidly related, and indeed in the bulk solution $v_{rms}/v_p \approx 1.24$ for both ions and is close to the Maxwell distribution value $(3/2)^{1/2} \approx 1.225$. Moreover, the relation of v_p to the ion mass $M = 2k_BT/v_p^2$ yields values close to the actual ion masses. However, in the membrane the ratio v_{rms}/v_p is significantly increased. Apparently, this indicates coexistence of two populations, a "slow" bulk-like one and a distinct population of faster ions. Superposition of two populations is what causes deviation of the v_{rms}/v_p ratio from the Maxwell distribution value. Figure 7 shows that the slow fraction is large enough to keep v_p unchanged, since the faster fraction has very few ions with this velocity; thus, the position of the maximum is preserved. On the other hand, the fast fraction adds significantly to the high-velocity tail of the distribution, which increases v_{rms}. Since the part of the box

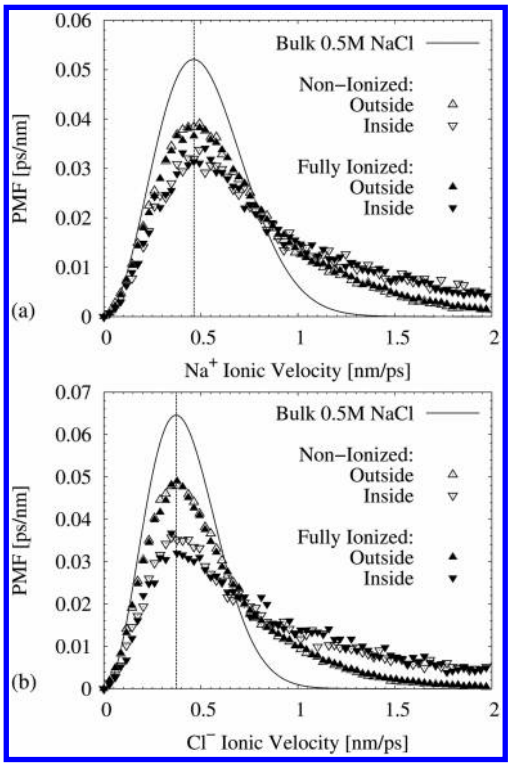

Figure 7. Probability mass function (PMF) of the ionic velocities of (a) Na^+ and (b) Cl^-.

Table 1. v_p and v_{rms} Velocities of Na^+ and Cl^- Calculated Using Equations 2 and 3 outside and inside the Neutral and Ionized Membranes and for 0.5 M NaCl Solution[a]

			nonionized membrane		fully ionized membrane	
ion	ionic velocity [nm/ps]	0.5 M NaCl solution	outside	inside	outside	inside
Na^+	v_p	0.46	0.46	0.47	0.46	0.46
	v_{rms}	0.57	0.79	0.92	0.77	0.91
Cl^-	v_p	0.37	0.37	0.37	0.38	0.37
	v_{rms}	0.46	0.64	0.87	0.65	0.89

[a]Prior to calculating v_p and v_{rms} the noise of the computed distributions was reduced using Chebyshev polynomials of degree 20.

DOI: 10.1021/acs.jpcb.5b06566
J. Phys. Chem. B XXXX, XXX, XXX−XXX

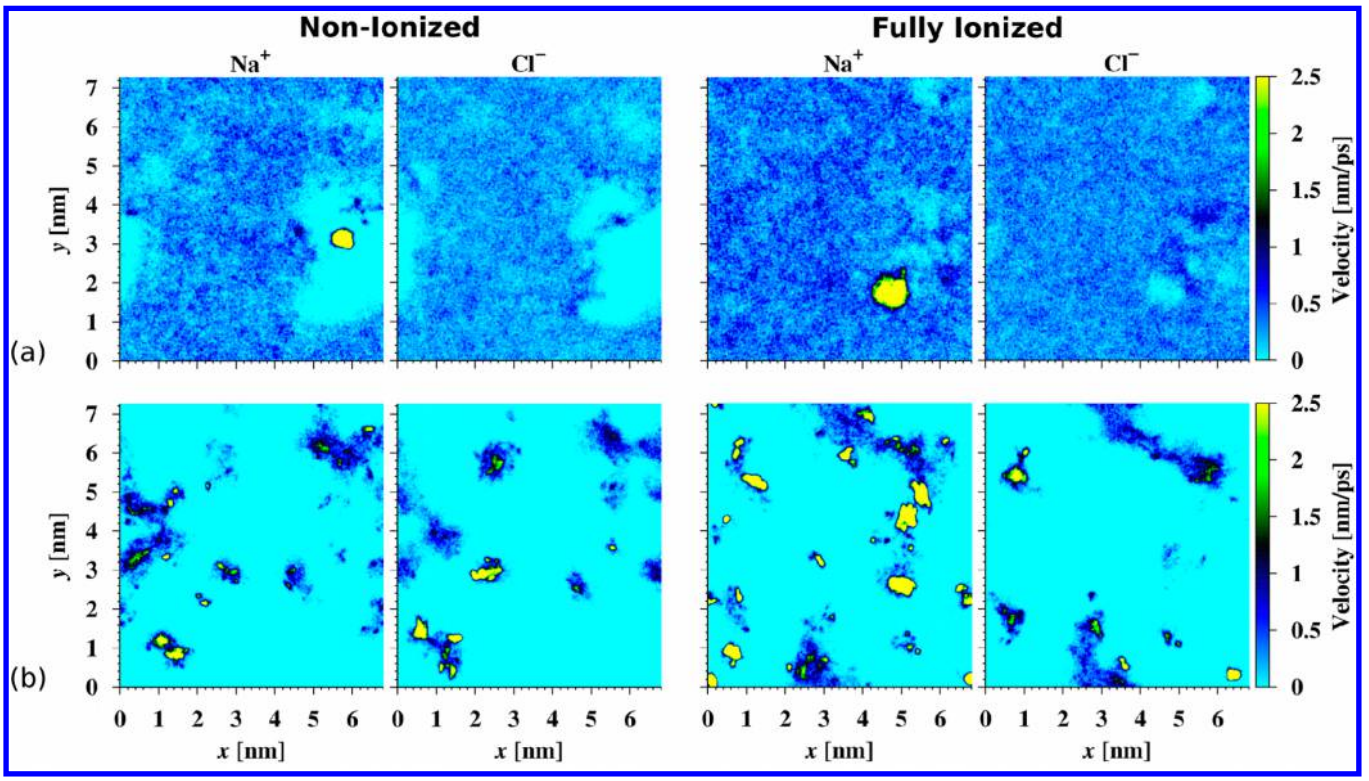

Figure 8. Local distribution of the atomic velocities of Na^+ and Cl^- ions (a) in solution next to polyamide water interface and (b) inside the polyamide membrane. The maps refer to the same slices as in Figure 3. Sections S6.3 and S6.4 of Supporting Information provide details on the plotting technique. See also Supporting Information video files.

defined as "outside of the membrane" also contains some polyamide, the effect appears both outside and inside the membrane, with the faster fraction being larger inside. Both inside and outside distributions are virtually identical for the nonionized and ionized membranes.

Figure 7 visualizes local variations of time-averaged ion velocities inside and outside the ionized and neutral membranes in the same manner and for the same representative slices, as the charge density maps in Figure 3. The dark blue color in Figure 8a indicates velocities similar to those in bulk solution (Figure 8b), while bright yellow color reveals much higher velocities within high ion density spots associated with fixed charges. Apparently, the electric field around the fixed charge accelerates the ions (electrophoretic effect[57]). Once trapped by a fixed charge, a counterion gains a significant kinetic energy and thereafter bounces elastically against the rigid surrounding matrix, preserving the high velocity but remaining strongly localized. Due to the localization, such fast-bouncing counterions are negligibly displaced over time and thus contribute little to ion diffusivity (see next).

Computing diffusivities is another way to analyze the dynamics of water and ions. An important difference from velocities is that molecules or ions have to show a significant displacement over time; thus, fast counterions bound to fixed charges contribute fairly little to diffusivity and transport across the entire membrane. Table 2 displays the scalar coefficient of self-diffusion, D, of water molecules and ions estimated from their mean squared displacement (MSD). The shown values were estimated by tracing only the particles (molecules of ions) which stayed inside the membrane 90% of the productive stage time. This increased the error ΔD by <15% but excluded the particles residing outside the membrane.

Table 2. Scalar Self-Diffusion Coefficient D and Its Standard Deviation ΔD Estimated for the SPC Water Molecules and Na^+ and Cl^- Ions in Nonionized and Ionized Membrane and in the Model 0.5 M NaCl Solution

	$D \pm \Delta D$ [$\times 10^{-9}$ m^2 s^{-1}]		
species	nonionized membrane	fully ionized membrane	0.5 M NaCl
SPC water	0.664 ± 0.022	0.556 ± 0.019	5.103 ± 0.048
Na^+	0.263 ± 0.092	0.122 ± 0.075	1.949 ± 0.125
Cl^-	0.324 ± 0.109	0.357 ± 0.198	1.837 ± 0.195

The diffusivity values for water are an order of magnitude lower than in the bulk and are consistent with previous MD estimates.[22,24,25] It was also most encouraging that the computed permeability was fairly consistent with the one actually measured. Indeed, assuming the solution-diffusion mechanism, a film of thickness δ = 100 nm, representative of dense commercial RO membranes, would have an osmotic (i.e., diffusive) water permeability $\phi_w D_w/\delta$, where $\phi_w \sim 0.2$[26] and $D_w \sim 0.6 \times 10^{-9}$ m^2 s^{-1} (Table 2) are the water volume fraction (partitioning coefficient) and diffusivity in polyamide. Further, assuming equivalence of osmotic and hydraulic pressures as the driving force for water transport, as standard in RO models, the diffusive permeability may be converted to hydraulic permeability L_p by the factor RT/V_w, where $V_w = 1.8 \times 10^{-5}$ m^3 mol^{-1} is the molar volume of water. The final expression is

$$L_p = \frac{RT}{V_w} \times \frac{\phi_w D_w}{\delta} \quad (4)$$

DOI: 10.1021/acs.jpcb.5b06566
J. Phys. Chem. B XXXX, XXX, XXX−XXX

Equation 4 yields a hydraulic permeability $L_p \sim 10^{-11}$ m s^{-1} Pa^{-1} or ∼1−10 L m^{-2} bar^{-1}, which is close to that of commercial membranes.

Table 2 shows that the average water mobility was somewhat larger for the neutral membrane, despite the fact that the ionized membrane should be slightly more hydrated. It is possible that the additional water hydrating the ionized groups could be localized and contributes insignificantly to water transport across the entire membrane. As the ultimate bottlenecks of the water transport across the membrane are water-lean passages separating water-rich pockets, larger hydration of isolated ionized sites increases the total water content but not as much water permeability, which means the average mobility per water molecule is reduced.

A similar effect may explain the variations of average mobility for Na^+ and Cl^- ions in different cases. Indeed, if the overall ion transport is determined by ion-lean fragments of polyamide, localized regions with higher ion concentration and mobility do not contribute significantly to the macroscopic ion transport. Thus, addition of ions to these regions should reduce the average ion mobility. This is what apparently happens when Na^+ content increases due to ionization of fixed charges. In contrast, ionization slightly reduces the Cl^- content (see below), as compared to the neutral polymer, and effective Cl^- mobility increases.

3.3. Effective Ion Sorption and Transport Characteristics of the Membrane. It is expedient to use the present results to estimate the effective or average salt transport and exclusion for the entire membrane, which are those that may be compared with experiment. The salt exclusion is transparently analyzed using the salt chemical potential μ_s or salt activity, $a_s = \exp(\mu_s/k_BT)$, which is related to the activities for univalent cations and anions a_+ and a_- and their concentrations in the membrane C_+ and C_- as follows:

$$a_s = a_+a_- = (\gamma_+\gamma_-)(C_+C_-) \tag{5}$$

For simplicity, the factors contributed to ionic activities by ion−ion interactions, will be ignored as a second-order effect, placing the focus on ion-membrane interactions, which is what mainly determines ion partitioning. Thus, as a reference, it is assumed that in solution $\gamma_+ \approx \gamma_- \approx 1$ and then $a_s \approx c_s^2$, where c_s is salt concentration in solution. Thereby the average product of activity coefficients in the membrane is given by $\gamma_+\gamma_- \approx c_s^2/(C_+C_-)$ and may be estimated from the computed values c_s and of C_+ and C_- averaged over the membrane. Thus, defined product $\gamma_+\gamma_-$ quantifies overall salt affinity to the membrane phase relative to solution, i.e., the non-Donnan contributions to salt exclusion,[53,54,58] since salt is overall neutral and the effect of Donnan potential is canceled out.

For the neutral membrane the product $\gamma_+\gamma_-$ has a straightforward relation to salt partitioning coefficient, that is, $K_s \equiv C_s/c_s = (\gamma_+\gamma_-)^{-1/2}$, where $C_s = C_+ = C_-$ is the free salt concentration in polyamide. Since the membrane is overall neutral, K_s is identical to the non-Donnan salt partitioning coefficient. The calculations summarized in Table 3 show that salt exclusion is relatively weak, $K_s = 0.26$ and $\gamma_+\gamma_- = 15.1$. This is still not as large as the RBS data of Zhang et al.[49] (this may have the same reason as higher salt permeability discussed below), but it emphasizes a much weaker exclusion than could be expected on the basis of physical properties of polyamide. For instance, one may compare these values to the Born equation used in the SDE model to describe the ion solvation contribution to non-Donnan partitioning[54,59]

Table 3. Values of C_+, C_-, $\gamma_+\gamma_-$, and K_s Computed with Respect to the Charge Content in the Active Part of the Membrane and Its Volume (See Figure 2)

ionization	X [M]	c_s [M]	C_+ [M]	C_- [M]	$\gamma_+\gamma_-$	K_s
none	0	0.66	0.17	0.17	15.1	0.26
full	0.5	0.93	0.66	0.16	8.1	0.17

$$\gamma_\pm^{\text{Born}} = \exp\left(\frac{\lambda_B}{2r_\pm}\right) \tag{5a}$$

where $r_\pm$ is the radius of the respective ion, either cation or anion. Apparently, the so-called Born ionic radii, 0.17 and 0.20 nm for Na^+ and Cl^-, respectively, are the most appropriate choice.[51] For λ_B of the order of a few nanometers (see section 3.1), this yields γ^{Born} above 10^3, meaning $K_s \leq 0.001$, which would also be more consistent with impedance spectroscopy.[60,61] However, as discussed in section 3.1, the actual mechanism of ion uptake and affinity to membrane reflected in $\gamma_+\gamma_-$ is strongly modified by the localized interaction with fixed charged sites. A high value of λ_B then promotes ion uptake rather than ion exclusion. Notably, the gain in electrostatic energy per such interaction in units of k_BT is of the order $\lambda_B/r_\pm$, just as the solvation energy in eq 5, but is negative (attraction). This attractive interaction reduces the solvation penalty and leads to a weak exclusion, i.e., smaller $\gamma_+\gamma_-$.

The picture is only slightly modified for the ionized membrane. When a genuine fixed charge of density X is introduced, the mean-field (Donnan) model predicts that the salt (i.e., co-ion) uptake should be reduced compared to the neutral membrane by a factor $(1 + (X/2c_s)^2\ \gamma_+\gamma_-)^{1/2} - (X/2c_s)(\gamma_+\gamma_-)^{1/2} < 1$.[54] The values obtained for ionized membrane and summarized in Table 3 show that, compared to neutral membrane, K_s is slightly reduced to 0.18, but $\gamma_+\gamma_-$ becomes smaller as well, i.e., salt affinity to the membrane increases and partly offsets the effect of X. This might be related to the contribution of fixed charges to affinity to Na^+, expressed by γ_+, since their charge is larger than that of atomic charges, and they compensate the unfavorable solvation energy to a larger degree. It is once again stressed that such compensation becomes possible due to the large value of the Bjerrum length which leads to localized sorption of mobile charges. These results seem to be consistent with and can explain relatively large values of K_s and fairly similar uptake of co- and counterions reported by Zhang et al.[49]

The data from Tables 2 and 3 may also estimate the effective intrinsic ion permeabilities (permeances) P_+ and P_- of Na^+ and Cl^-, as follows for nonionized membrane:

$$P_+ = \frac{D_+C_+}{c_s} = \frac{0.263 \times 10^{-9} \times 0.17}{0.66} = 6.76 \times 10^{-11}\ \text{m}^2/\text{s}$$

$$P_- = \frac{D_-C_-}{c_s} = \frac{0.324 \times 10^{-9} \times 0.17}{0.66} = 8.32 \times 10^{-11}\ \text{m}^2/\text{s}$$

Similarly, for fully ionized membrane

$$P_+ = \frac{0.122 \times 10^{-9} \times 0.66}{0.93} = 8.64 \times 10^{-11}\ \text{m}^2/\text{s}$$

$$P_- = \frac{0.367 \times 10^{-9} \times 0.16}{0.93} = 6.40 \times 10^{-11}\ \text{m}^2/\text{s}$$

DOI: 10.1021/acs.jpcb.5b06566
J. Phys. Chem. B XXXX, XXX, XXX−XXX

Taking δ = 100 nm as a representative thickness these values may be used to compute the salt permeability ω_s of an RO membrane, nonionized

$$\omega_s = \frac{P_s}{\delta} = \frac{2}{\delta}\left(\frac{1}{P_+} + \frac{1}{P_-}\right)^{-1} = 0.746 \times 10^{-3}\ \mathrm{m/s}$$

and fully ionized,

$$\omega_s = \frac{P_s}{\delta} = \frac{2}{\delta}\left(\frac{1}{P_+} + \frac{1}{P_-}\right)^{-1} = 0.736 \times 10^{-3}\ \mathrm{m/s}$$

This may be compared to the typical salt permeability of dense RO membranes, which is of the order 10^{-7} m/s,[60] i.e., about 4 orders of magnitude smaller than present results.

Such a large discrepancy between measured and computed permeabilities may seem surprising, given the assembled polyamide composition and computed ion and water uptake and water permeability agreed with the measured ones. We believe that this result indicates that the model structure used here was too uniform and thus largely underestimated the barrier properties of polyamide toward ions. For instance, for the given composition a much lower polyamide permeability could be obtained, if the water-rich cavities were substantially larger but were fully enclosed by dense polymer. Indeed, recently, there has been compelling evidence that polyamide membranes, even the densest ones, may contain a significant water-filled void fraction;[3,62,63] thus, the average composition, e.g., measured by RBS, may be misleading. Taking the density maps in Figure 3 as an example, ion-free dense polyamide fragments encircled with a red dashed line in Figure 3b do not form a continuous barrier. Thus, ions can travel across the loosely connected network of water-filled pores relatively fast. In a real membrane such dense fragments may be much thicker and form continuous and nearly impermeable barriers between larger cavities.

One reason why such a structure was not obtained in this study may be traced back to the limitation on the system size, time, and anisotropy during polymer assembly, which could affect the scale and magnitude of compositional fluctuations in the forming film. The latter are known to correlate with the film thickness[4] and were apparently much smaller in the present case that in a larger real system, resulting in a dramatic difference in ion permeability. On the other hand, ion-free fragments are still hydrated and water-permeable (see water panels in Figure 3b); therefore, there was not such a large discrepancy for water permeability.

4. CONCLUSIONS

The present study highlights benefits and limitations of MD simulations for gaining insights and quantitative estimates of ion uptake and dynamics in polyamide desalination membranes. Simulations demonstrate that the mechanism of ion uptake distinctly differs from what mean-field approaches usually assume. In particular, the concept of a smeared Donnan potential breaks down, and ion sorption on charged sites in the membrane phase appears to be highly localized, owing to the dominance of electrostatic forces over translational entropy of the ions, as indicated by a large Bjerrum length. For this reason, sorption on partial atomic charges becomes possible, and thus, co-ion sorption in a charged membrane is greatly enhanced compared to the Donnan-related models, such as SDE. As a result, the effect of fixed charges on salt exclusion weakens, and the difference between neutral and charged membranes become fairly minor. This mechanism could explain the unexpectedly high ion uptake measured in polyamide membranes[49,50] and puzzling variations of ion sorption and permeation at low salt concentrations.[53−55]

On the other hand, the MD simulations greatly overestimate ion and salt permeability, despite the observation that the average chemical composition and water permeability match well those of genuine polyamide membranes. A likely reason is the relative uniformity of the model membrane used here, in which the small scale and magnitude of density and compositional fluctuations result in a good connectivity of the water- and ion-rich regions and allow fast ion permeation past very dense ion-free fragment of polyamide. In real membranes such dense polyamide may form continuous barriers that cannot be as easily bypassed through more permeable regions. In such a case, ion sorption and permeation will be essentially decoupled. Even when disconnected, looser regions may significantly contribute to ion sorption, like in the present simulations, yet they would not contribute as much to the ion permeation, which will be determined by the dense barriers.

It may then be of significant interest to assess the water and ion uptake and permeability of dense polyamide fragments as more representative of barrier properties of polyamide. Unfortunately, even for such a large structure as the one analyzed here, the amount of ions in the dense fragments is too small for a sensible analysis. This suggests that MD might not be able to supply all the answers, which may have to rely on other methods, such as analytical theories and new experiments.

■ ASSOCIATED CONTENT

Supporting Information

The Supporting Information is available free of charge on the ACS Publications website at DOI: 10.1021/acs.jpcb.5b06566.

Sections S1−6 detailing computational routines; water settling, salination, ionization protocol, and equilibration protocols; and grid spacial statistics routine (PDF)

Video showing atomic charge variation across the nonionized polyamide membrane (QT)

Video showing atomic charge variation across the fully ionized polyamide membrane (QT)

Video showing ionic velocity and charge variation across the nonionized polyamide membrane (QT)

Video showing ionic velocity and charge variation across the fully ionized polyamide membrane (QT)

■ AUTHOR INFORMATION

Corresponding Author

*E-mail: vfreger@tx.technion.ac.il.

Notes

The authors declare no competing financial interest.

■ ACKNOWLEDGMENTS

The authors acknowledge financial support by the Israeli Science Foundation, Grant 1152/11.

■ REFERENCES

(1) Petersen, R. J. Composite Reverse Osmosis and Nanofiltration Membranes. *J. Membr. Sci.* **1993**, *83*, 81−150.

(2) Drioli. E.; Giorno, L. *Comprehensive Membrane Science and Engineering*; Elsevier Science: Amsterdam, 2010.

DOI: 10.1021/acs.jpcb.5b06566
J. Phys. Chem. B XXXX, XXX, XXX−XXX

(3) Freger, V. Nanoscale Heterogeneity of Polyamide Membranes Formed by Interfacial Polymerization. *Langmuir* **2003**, *19*, 4791−4797.
(4) Freger, V. Kinetics of Film Formation by Interfacial Polycondensation. *Langmuir* **2005**, *21*, 1884−1894.
(5) Arthur, S. D. Structure-Property Relationship in a Thin Film Composite Reverse Osmosis Membrane. *J. Membr. Sci.* **1989**, *46*, 243−260.
(6) Sundet, S. A. Morphology of the Rejecting Surface of Aromatic Polyamide Membranes for Desalination. *J. Membr. Sci.* **1993**, *76*, 175−183.
(7) Chai, G.; Krantz, W. B. Formation and Characterization of Polyamide Membranes via Interfacial Polymerization. *J. Membr. Sci.* **1994**, *93*, 175−192.
(8) Hirose, M.; Minamizaki, Y.; Kamiyama, Y. The Relationship Between Polymer Molecular Structure of RO Membrane Skin Layers and Their RO Performances. *J. Membr. Sci.* **1997**, *123*, 151−156.
(9) Kwak, S.; Jung, S. G.; Kim, S. H. Structure-Motion-Performance Relationship of Flux-Enhanced Reverse Osmosis (RO) Membranes Composed of Aromatic Polyamide Thin Films. *Environ. Sci. Technol.* **2001**, *35*, 4334−4340.
(10) Freger, V. Swelling and Morphology of the Skin Layer of Polyamide Composite Membranes: An Atomic Force Microscopy Study. *Environ. Sci. Technol.* **2004**, *38*, 3168−3175.
(11) Cahill, D. G.; Freger, V.; Kwak, S. Microscopy and Microanalysis of Reverse-Osmosis and Nanofiltration Membranes. *MRS Bull.* **2008**, *33*, 27−32.
(12) Coronell, O.; Mariñas, B. J.; Cahill, D. G. Accessibility and Ion Exchange Stoichiometry of Ionized Carboxylic Groups in the Active Layer of FT30 Reverse Osmosis Membrane. *Environ. Sci. Technol.* **2009**, *43*, 5042−5048.
(13) Zhang, X.; Cahill, D. G.; Coronell, O.; Mariñas, B. J. Absorption of Water in the Active Layer of Reverse Osmosis Membranes. *J. Membr. Sci.* **2009**, *331*, 143−151.
(14) Coronell, O.; Mariñas, B. J.; Cahill, D. G. Depth Heterogeneity of Fully Aromatic Polyamide Active Layers in Reverse Osmosis and Nanofiltration Membranes. *Environ. Sci. Technol.* **2011**, *45*, 4513−4520.
(15) Kim, S. H.; Kwak, S.; Suzuki, T. Positron Annihilation Spectroscopic Evidence to Demonstrate the Flux-Enhancement Mechanism in Morphology-Controlled Thin-Film-Composite (TFC) Membrane. *Environ. Sci. Technol.* **2005**, *39*, 1764−1770.
(16) Freger, V.; Srebnik, S. Mathematical Model of Charge and Density Distributions in Interfacial Polymerization of Thin Films. *J. Appl. Polym. Sci.* **2003**, *88*, 1162−1169.
(17) Yashin, V. V.; Balazs, A. C. Theoretical Model of Interfacial Polymerization. *J. Chem. Phys.* **2004**, *121*, 11440−11454.
(18) Berezkin, A. V.; Khokhlov, A. R. Mathematical Modeling of Interfacial Polycondensation. *J. Polym. Sci., Part B: Polym. Phys.* **2006**, *44*, 2698−2724.
(19) Ebro, H.; Kim, Y. M.; Kim, J. H. Molecular Dynamics Simulations in Membrane-Based Water Treatment Processes: A Systematic Overview. *J. Membr. Sci.* **2013**, *438*, 112−125.
(20) Kotelyanskii, M. J.; Wagner, N. J.; Paulaitis, M. E. Atomistic Simulation of Water and Salt Transport in the Reverse Osmosis Membrane FT-30. *J. Membr. Sci.* **1998**, *139*, 1−16.
(21) Kotelyanskii, M. J.; Wagner, N. J.; Paulaitis, M. E. Molecular Dynamics Simulation Study of the Mechanisms of Water Diffusion in a Hydrated, Amorphous Polyamide. *Comput. Theor. Polym. Sci.* **1999**, *9*, 301−306.
(22) Harder, E.; Walters, D. E.; Bodnar, Y. D.; Faibish, R. S.; Roux, B. Molecular Dynamics Study of a Polymeric Reverse Osmosis Membrane. *J. Phys. Chem. B* **2009**, *113*, 10177−10182.
(23) Luo, Y.; Harder, E.; Faibish, R. S.; Roux, B. Computer Simulations of Water Flux and Salt Permeability of the Reverse Osmosis FT-30 Aromatic Polyamide Membrane. *J. Membr. Sci.* **2011**, *384*, 1−9.
(24) Hughes, Z. E.; Gale, J. D. A Computational Investigation of the Properties of a Reverse Osmosis Membrane. *J. Mater. Chem.* **2010**, *20*, 7788−7799.
(25) Ding, M.; Szymczyk, A.; Goujon, F.; Soldera, A.; Ghoufi, A. Structure and Dynamics of Water Confined in a Polyamide Reverse-Osmosis Membrane: A Molecular-Simulation Study. *J. Membr. Sci.* **2014**, *458*, 236−244.
(26) Kolev, V.; Freger, V. Hydration, Porosity and Water Dynamics in the Polyamide Layer of Reverse Osmosis Membranes: A Molecular Dynamics Study. *Polymer* **2014**, *55*, 1420−1426.
(27) Bekker, H.; Berendsen, H. J. C.; Dijkstra, E. J.; Achterop, S.; van Drunen, R.; van der Spoel, D.; Sijbers, A.; Keegstra, H.; Reitsma, B.; Renardus, M. K. R. Gromacs: A Parallel Computer for Molecular Dynamics Simulations. In *Physics Computing 92 (Singapore, 1993)*; de Groot, R. A., Nadrchal, J., Eds.; World Scientific: Singapore, 1993.
(28) Berendsen, H. J. C.; van der Spoel, D.; van Drunen, R. GROMACS: A Message-Passing Parallel Molecular Dynamics Implementation. *Comput. Phys. Commun.* **1995**, *91*, 43−56.
(29) Lindahl, E.; Hess, B.; van der Spoel, D. GROMACS 3.0: A Package for Molecular Simulation and Trajectory Analysis. *J. Mol. Mod.* **2001**, *7*, 306−317.
(30) van der Spoel, D.; Lindahl, E.; Hess, B.; Groenhof, G.; Mark, A. E.; Berendsen, H. J. C. GROMACS: Fast, Flexible and Free. *J. Comput. Chem.* **2005**, *26*, 1701−1718.
(31) Hess, B.; Kutzner, C.; van der Spoel, D.; Lindahl, E. GROMACS 4: Algorithms for Highly Efficient, Load-Balanced, and Scalable Molecular Simulation. *J. Chem. Theory Comput.* **2008**, *4*, 435−447.
(32) Wang, J.; Wolf, R. M.; Caldwell, J. W.; Kollman, P. A.; Case, D. A. Development and Testing of a General Amber Force Field. *J. Comput. Chem.* **2004**, *25*, 1157−1174.
(33) Jørgensen, W. L.; Chandrasekhar, J.; Madura, J. D.; Impey, R. W.; Klein, M. L. Comparison of Simple Potential Functions for Simulating Liquid Water. *J. Chem. Phys.* **1983**, *79*, 926−935.
(34) Berendsen, H. J. C.; Postma, J. P. M.; van Gunsteren, W. F.; Hermans, J. Simple Point Charge Water. In *Intermolecular Forces*; Pullman, B., Ed.; Reidel: Dordrecht, 1981; p 331.
(35) Knecht, V.; Klasczyk, B.; Dimova, R. Macro- Versus Microscopic View of the Electrokinetics of a Water-Membrane Interface. *Langmuir* **2013**, *29*, 7939−7948.
(36) Chen, A. A.; Pappu, R. V. Parameters of Monovalent Ions in the AMBER-99 Force Field: Assessment of Inaccuracies and Proposed Improvements. *J. Phys. Chem. B* **2007**, *111*, 11884−11887.
(37) Berendsen, H. J. C.; Postma, J. P. M.; van Gunsteren, W. F.; DiNola, A.; Haak, J. R. Molecular Dynamics with Coupling to an External Bath. *J. Chem. Phys.* **1984**, *81*, 3684−3690.
(38) Parrinello, M.; Rahman, A. J. Polymorphic Transitions in Single Crystal: A New Molecular Dynamics Method. *J. Appl. Phys.* **1981**, *52*, 7182−7190.
(39) Chandler, D. *Introduction to Modern Statistical Mechanics*; Oxford University Press: Oxford, U.K., 1987.
(40) Bayly, C.; Cieplak, P.; Cornell, W.; Kollman, P. A Well-Behaved Electrostatic Potential Based Method Using Charge Restraints for Deriving Atomic Charges: The RESP Model. *J. Phys. Chem.* **1993**, *97*, 10269−10280.
(41) Cieplak, P.; Cornell, W.; Bayly, C.; Kollman, P. Application of the Multimolecule and Multiconformational RESP Methodology to Biopolymers: Charge Derivation for DNA, RNA, and Proteins. *J. Comput. Chem.* **1995**, *16*, 1357−1377.
(42) Barr, S.; Panagiotopoulos, A. Interactions Between Charged Surfaces with Ionizable Sites. *Langmuir* **2011**, *27*, 8761−8766.
(43) Argyris, D.; Cole, D.; Striolo, A. Ion-Specific Effects Under Confinement: The Role of Interfacial Water. *ACS Nano* **2010**, *4*, 2035−2042.
(44) Bonnaud, P.; Coasne, B.; Pellenq, R. Solvated Calcium Ions in Charged Silica Nanopores. *J. Chem. Phys.* **2012**, *137*, 64706−64712.
(45) Renou, R.; Szymczyk, A.; Ghoufi, A. Water Confinement in Nanoporous Silica Materials. *J. Chem. Phys.* **2014**, *140*, 44704−44708.
(46) Yang, K. L.; Yiacoumi, S.; Tsouris, C. Electrical Double-Layer Formation. In *Decker Encyclopedia of Nanoscience and Nanotechnology*; Schwarz, J., Contescu, C., Ed.; CRC Press: Boca Raton, FL, 2004.

DOI: 10.1021/acs.jpcb.5b06566
J. Phys. Chem. B XXXX, XXX, XXX−XXX

(47) Aparicio, S.; Atilhan, M. A Computational Study on Choline Benzoate and Choline Salicylate Ionic Liquids in the Pure State and After CO2 Adsorption. *J. Phys. Chem. B* **2012**, *116*, 9171−9185.
(48) Bruni, L.; Bandini, S. The Role of the Electrolyte on the Mechanism of Charge Formation in Polyamide Nanofiltration Membranes. *J. Membr. Sci.* **2008**, *308*, 136−151.
(49) Zhang, X. J.; Cahill, D. G.; Coronell, O.; Marinas, B. J. Partitioning of Salt Ions in FT30 Reverse Osmosis Membranes. *Appl. Phys. Lett.* **2007**, *91*, 181904.
(50) Toubeli, A.; Kiparissides, C. Synthesis and Characterization of Polyterephthalamide Membranes for Encapsulation Use: Effect of the Amine Type and Composition on the Membrane Permeability. *J. Membr. Sci.* **1998**, *146* (1), 15−29.
(51) Mancinelli, R.; Botti, A.; Bruni, F.; Ricci, M. A.; Soper, A. K. Hydration of Sodium, Potassium, and Chloride Ions in Solution and the Concept of Structure Maker/Breaker. *J. Phys. Chem. B* **2007**, *111*, 13570−13577.
(52) Lyubartsev, A. P.; Laaksonen, A. Concentration Effects in Aqueous NaCl Solutions. A Molecular Dynamics Simulation. *J. Phys. Chem.* **1996**, *100*, 16410−16418.
(53) Bason, S.; Kaufman, Y.; Freger, V. Analysis of Ion Transport in Nanofiltration Using Phenomenological Coefficients and Structural Characteristics. *J. Phys. Chem. B* **2010**, *114*, 3510−3517.
(54) Bason, S.; Freger, V. Phenomenological Analysis of Transport of Mono- and Divalent Ions in Nanofiltration. *J. Membr. Sci.* **2010**, *360*, 389−396.
(55) Galama, A. H.; Post, J. W.; Stuart, M. A. C.; Biesheuvel, P. M. Validity of the Boltzmann Equation to Describe Donnan Equilibrium at the Membrane−Solution Interface. *J. Membr. Sci.* **2013**, *442*, 131−139.
(56) Ben-David, A.; Bason, S.; Jopp, J.; Oren, Y.; Freger, V. Partitioning of Organic Solutes Between Water and Polyamide Layer of RO and NF Membranes: Correlation to Rejection. *J. Membr. Sci.* **2006**, *281*, 480−490.
(57) Hu, Z.; Jiang, J. Electrophoresis in Protein Crystal: Non-equilibrium Molecular Dynamics Simulations. *Biophys. J.* **2008**, *95*, 4148−4156.
(58) Yaroshchuk, A.; Karpenko, L.; Ribitsch, V. Measurements of Transient Membrane Potential After Current Switch-off as a Tool to Study the Electrochemical Properties of Supported Thin Nanoporous Layers. *J. Phys. Chem. B* **2005**, *109*, 7834−7842.
(59) Szymczyk, A.; Fatin-Rouge, N.; Fievet, P.; Ramseyer, C.; Vidonne, A. Identification of Dielectric Effects in Nanofiltration of Metallic Salts. *J. Membr. Sci.* **2007**, *287*, 102−110.
(60) Bason, S.; Oren, Y.; Freger, V. Characterization of Ion Transport in Thin Films Using Electrochemical Impedance Spectroscopy: II: Examination of the Polyamide Layer of RO Membranes. *J. Membr. Sci.* **2007**, *302*, 10−19.
(61) Bason, S.; Oren, Y.; Freger, V. Ion transport in the Polyamide Layer of RO Membranes: Composite Membranes and Free-Standing Films. *J. Membr. Sci.* **2011**, *367*, 119−126.
(62) Pacheco, F. 3D Visualization of the Internal Nanostructure of Polyamide Thin Films in RO Membranes. In *Proceedings of ICOM 2015 International Congress on Membranes*; Suzhou, China, July 21−25, 2014.
(63) Lin, L.; Lopez, R.; Ramon, G. Z.; Coronell, O. Investigating the Void Structure of the Polyamide Active Layers of Thin-Film Composite Membranes. *J. Membr. Sci.* **2016**, *497*, 365−376.

DOI: 10.1021/acs.jpcb.5b06566
J. Phys. Chem. B XXXX, XXX, XXX−XXX